Journal of Catalysis **211,** 451–463 (2002)
doi:10.1006/jcat.2002.3750

Carbon–Chlorine and Carbon–Bromine Bond Cleavage in the Catalytic Hydrodehalogenation of Halogenated Aromatics

Colin Park,* Claudia Menini,* Jose Luis Valverde,† and Mark A. Keane‡,[1]

*Department of Chemical Engineering, University of Leeds, Leeds LS2 9JT, United Kingdom; †Departamento de Ingenieria Quimica, Universidad de Castilla La Mancha, 13004 Ciudad Real, Spain; and ‡Department of Chemical and Materials Engineering, University of Kentucky, Lexington, Kentucky 40506-0046

Received April 8, 2002; revised July 16, 2002; accepted July 17, 2002

The catalytic hydrodehalogenation of chlorobenzene (CB), bromobenzene (BB), CB/BB mixtures, and the three chlorobromobenzene (CBB) isomers was studied over the temperature range 473 K ≤ $T \leq 603$ K using Ni/SiO_2 where the Ni loading was varied from 6.2 to 15.2% wt/wt. Each catalyst was 100% selective in terms of hydrodehalogenation and there was no evidence of any aromatic ring reduction. Steady-state conversion was readily achieved but there was a decided decline in activity with prolonged catalyst use. The catalyst samples were characterized, before and after use, by TEM, CO chemisorption/TPD, TPO, and potentiometric analysis. We recorded the levels of reversibly and irreversibly held Cl and/or Br on the spent catalysts. Appreciable Ni particle growth during catalysis was observed and this is attributed to a halide-induced metal agglomeration, while CO TPD revealed a significant disruption to the Ni particle electronic structure. Long-term deactivation is ascribed to a less effective activation of the haloarene and/or hydrogen reactant(s) allied to a halide-promoted carbonaceous deposition; the surface coke is characterized as predominantly amorphous. Reactivity increased in the order 2-CBB < 3-CBB < 4-CBB < BB < CB, which is taken to be diagnostic of an electrophilic mechanism where the presence of a second electron withdrawing a halogen substituent lowers the overall dehalogenation rate and steric hindrance governs reactivity in the case of the CBB isomers. In the hydrotreatment of CB/BB mixtures and CBB isomers, the fractional debromination increased due to a surface hydrochlorination and Cl exchange with the Br substituent on the aromatic ring. The reaction orders with respect to CB, BB, and H_2 were determined, while the experimentally determined rate/pressure profiles were subjected to standard Langmuir–Hinshelwood kinetic modeling. The best overall (meaningful) fit to the experimental data was achieved with a model based on the associative adsorption of the haloarene and the dissociative adsorption of hydrogen on the same sites with no product inhibition.

Key Words: **catalytic hydrodehalogenation; chlorobenzene; bromobenzene; chlorobromobenzene; nickel/silica.**

INTRODUCTION

Halogenated organics are persistent toxic compounds (1, 2) for which the environment has little assimilative capacity. Catalytic hydrodehalogenation represents a nondestructive means of treating halogenated waste that facilitates product recycling with a lower net impact on the environment (3–6). Chlorinated benzenes have emerged as a favored model feedstock to probe fundamental aspects of hydrodehalogenation, as they are representative of halogenated species typically found in organic waste. The catalysts that have been studied include an array of monometallic (principally Pt, Pd, and Ni) and bimetallic (Pt/Rh and Ni/Mo) systems (6–13). This report focuses on the application of silica-supported Ni in the gas phase, a catalytic system that has not been studied to any great extent. Hagh and Allen (10) have examined gas-phase hydrodehalogenation kinetics for chlorobenzene and 1,2-dichlorobenzene over $NiMo/\gamma Al_2O_3$ where the catalyst showed high dechlorination activity and no appreciable hydrogenation of the aromatic ring was detected. Suzdorf *et al.* (11) studied the effect of a range of ring substituents on hydrodechlorination activity and classified the reaction as an electrophilic substitution. Estelle *et al.* (12), in examining the gas-phase dechlorination of *ortho*-dichlorobenzene over unsupported Ni, showed that the reaction is structure sensitive. More recently, Cesteros *et al.* (13, 14) have reported high selectivities in terms of benzene formation from the gas-phase hydrodechlorination of 1,2,4-trichlorobenzene over $Ni/NiAl_2O_4$ and Ni/Mg/Al hydrotalcite systems.

By comparison, the treatment of bromobenzenes has received scant attention and few published accounts could be found. Wei *et al.* (15), in a homogeneous application, have used metallocenyl diphosphine complexes for the liquid-phase debromination of hexabromobenzene and generated mixtures of bromobenzene, dibromobenzenes, and tribromobenzenes. Palladium supported on $SiO_2/AlPO_4$, ZrO_2, and MgO was found to be active in the liquid-phase hydrodebromination of bromobenzene (16) while Yu *et al.* (17)

[1] To whom correspondence should be addressed. Fax: +1 (859) 3231929. E-mail: makeane@engr.uky.edu.

0021-9517/02 $35.00

employed PVP–$PdCl_2$ catalysts (PVP = poly(*N*-vinyl-2-pyrrolidone) and observed a catalyst poisoning by the HBr product. Indeed, catalyst deactivation appears to be a crucial issue in the treatment of chlorinated aliphatic (18) and aromatic (14, 19) reactants. Halogens are known to act as strong poisons in the case of transition metal catalysts (12, 18–21). Ohtsuka (20) has studied the influence of HCl treatment on the dispersion of Ni particles supported on carbon and noted a sintering of the Ni phase that was attributed to an agglomeration of mobile Ni–Cl species. Deactivation has been ascribed to different causes ranging from deposition of coke (6) to the formation of surface metal halides (12, 18, 21) to sintering (20) but no conclusive deactivation mechanism has yet emerged. In this study, we have considered the gas-phase hydrodehalogenation of chlorobenzene (CB), bromobenzene (BB), CB/BB mixtures, and the three chlorobrobenzene (CBB) isomers over Ni/SiO_2 of varying Ni loading (6.2–15.2% wt/wt). We address herein the nature of haloarene reactivity, mechanistic and kinetic features of hydrodehlogenation, and catalyst deactivation, providing characterization results for the catalysts before and after use.

EXPERIMENTAL

Catalyst Preparation, Activation, and Characterization

Three silica-supported nickel (6.2, 11.9, and 15.2% wt/wt Ni) precursors were prepared by homogeneous precipitation/deposition (23). Bulk Ni content in the activated catalysts before and after use was determined (to within ±2%) by atomic absorption spectrophotometry (Varian Spectra AA-10): the samples were first digested in HF (37% concentration) overnight at room temperature. The hydrated catalyst precursors, sieved in the 150- to 200-μm-mesh range, were reduced without a precalcination step, by heating in a 100 $cm^3\ min^{-1}$ stream of purified H_2 at a fixed rate (5 K min^{-1}, controlled using a Eurotherm 91e temperature programmer) to a final temperature of 673 ± 1 K, which was maintained for 18 h. The activated catalysts were also pretreated by contact with flowing HCl or HBr gas (20–150 $cm^3\ min^{-1}$ for 0.25–5 min) at 548 K; HCl/HBr contact was accompanied by an increase in the catalyst bed temperature by up to 34 K. Room temperature CO chemisorption was employed to characterize the supported Ni in the freshly activated and used catalysts. The samples were activated as above and then cooled to 298 K in dry He, and a fixed volume (10 μl) of CO was pulsed into the He carrier gas stream, where the concentration of CO exiting the reactor was measured using an online thermal conductivity detector (TCD) in conjunction with the JCL6000 (for Windows) data collection/manipulation package. The injection of CO was repeated until the downstream peak area was constant, indicating surface saturation with CO. The samples were thoroughly flushed with dry He (100 $cm^3\ min^{-1}$) for 1 h to remove any physisorbed CO. The catalyst then underwent a temperature ramp (25 K min^{-1}) in dry He (75 $cm^3\ min^{-1}$) to 1073 K, with the exiting gas stream passing through the online TCD to generate the CO TPD profile. The catalyst bed temperature was independently monitored via an online data logging system (Pico Technology, model TC-08). Upon completion of the CO TPD sequence, a series of calibration test peaks were taken to quantify CO uptake; reproducibility was better than ±3%. The desorption characteristics of CB from freshly activated and deactivated 6.2% wt/wt Ni/SiO_2 were studied, where the unused and spent samples were activated as above and then contacted at 573 K with 0.015 mol CB in a stream of dry H_2 (75 $cm^3\ min^{-1}$). The temperature was maintained for a further 30 min to remove any weakly held chlorobenzene before cooling to room temperature in dry He (75 $cm^3\ min^{-1}$); a subsequent temperature ramp (10 K min^{-1}) to 873 K in dry He with online TCD analysis of the effluent gas facilitated construction of the TPD profiles.

Transmission electron microscopy (TEM) analysis was carried out using a Philips CM200 FEGTEM operated at an accelerating voltage of 200 keV. The specimens were prepared by ultrasonic dispersion in 2-butanol, evaporating a drop of the resultant suspension onto a holey carbon-support grid. The particle size distribution profiles presented in this study are based on a measurement of over 500 individual particles.

Catalytic Reactor System/Kinetic Modeling

All catalytic reactions were carried out under atmospheric pressure, *in situ* immediately following the activation step, in a fixed-bed reactor over the temperature range 473 K $\leq T \leq$ 603 K. The catalysis procedure has been described in some detail elsewhere (24) but some features, pertinent to this study, are given below. A Model 100 (kd Scientific) microprocessor-controlled infusion pump was used to deliver the halogenated feed via a glass/PTFE gastight syringe and PTFE line at a fixed, calibrated, rate. The vaporized reactant was carried through the catalyst bed in a stream of dry H_2 and/or He, the flow rate of which was monitored using a Humonics (Model 520) digital flow meter. Undiluted chlorobenzene (CB; Aldrich, 99%) and bromobenzene (BB; Aldrich, 99%) and solutions of 2-chlorobromobenzene (2-CBB), 3-chlorobromobenzene (3-CBB), and 4-chlorobromobenzene (4-CBB; Aldrich 99%) in methanol (Aldrich, 99.8%) and *n*-hexane (Aldrich, 95+%) served as feedstock, where the inlet aromatic molar feed rate (F_{in}) was in the overall range 5.7×10^{-5}–6.7×10^{-3} mol h^{-1}. Mixtures of CB and BB in methanol and *n*-hexane were also treated, where the total molar halogen flow was maintained at 1.7×10^{-4} mol h^{-1}. Passage of each reactant/solvent combination in a stream of H_2 through the

empty reactor over the range of process temperatures did not result in any detectable conversion. The catalytic measurements were made at a gas space velocity of 2250 h^{-1} and at W/F_{in} values in the range 75–8772 $g\,h^{-1}\,mol^{-1}$, where W is the weight of activated catalyst. Mass diffusion contributions under these conditions are negligible; effectiveness parameter (25) at 573 K > 0.99. The rate data were likewise exempt from heat transport artifacts and calculation of inter- and intraparticle heat transfer coefficients (26) revealed that the temperature differential between the catalyst particle and the bulk fluid phase was <1 K. In the kinetic studies, the H_2 partial pressure was varied (from 0.36 to 0.96 atm) by dilution in He, while the haloaromatic pressures were within the range 0.0004–0.08 atm. Seven standard Langmuir–Hinshelwood expressions were tested, where parameter estimation was performed via minimization of the sum of residual squares in reaction rates using the Marquardt–Levenberg algorithm (27–29). Discrimination between the kinetic models tested was made by considering (i) the minimum values of both the sum of residual squares (χ^2) and the average relative percentage error (ε) and (ii) an F-test based on the ratio

$$F_c = \frac{\text{regression sum of squares/parameter number}}{\text{residual sum of squares/degree of freedom}}.$$

A given regression was deemed meaningful when the ratio

$$\frac{F_c}{F(\text{parameter number, degree of freedom}, 1-\alpha)}$$

was greater than unity. In this work, an α value of 0.05 was applied; a complete treatment of this statistical analysis is available elsewhere (28).

The reactor effluent was frozen in a liquid nitrogen trap and analyzed by capillary chromatography as described previously (24). One standard set of process conditions (CB feed, $T = 523$ K, and $W/F_{in} = 170\ g\,h^{-1}\,mol^{-1}$) was routinely repeated to ensure that the catalyst had not suffered any long-term deactivation. Molar percentage selectivity (S) in terms of product x is defined as $m_x/m_{tot} \times 100$, where m_{tot} is the total number of moles of product in the effluent stream; product composition was reproducible to better than ±7%. A halogen mass balance was performed by bubbling the effluent gas through an aqueous NaOH ($3.5–8.0\times10^{-3}$ mol dm^{-3} kept under constant agitation at 400 rpm) trap, with the halogen content quantitatively monitored by a Metrohm (Model 728) Autotitrator ($AgNO_3$ titrant, combined Ag electrode); mass balance was complete to within ±10%. A qualitative analysis (24) of the scrubbing solution for the presence of Cl_2 or Br_2 proved negative in every instance, indicating that the hydrogen halide was the sole inorganic product. In a separate set of experiments, the residual "reversibly" and "irreversibly" held halogen component on the catalyst after use was determined. The hydrodehalogenation of CB, BB, 2-CBB, and an equimolar mixture of CB/BB was conducted over freshly activated Ni/SiO_2 under identical conditions: $T = 603$ K; total feed hydroprocessed, 5.8×10^{-3} mol. The feed was cut and the catalyst swept with dry H_2 at 60 $cm^3\ min^{-1}$ for 1 h at 603 K. The reversibly held halogen component was desorbed from the catalyst by TPD (10 K min^{-1} to 723 K) with an isothermal hold at the final temperature for 16 h. The effluent stream was trapped in the NaOH scrubbing solution and the halogen content determined as described above. The irreversibly held halogen content was then measured by heating a known weight (ca. 0.2 g) of the spent catalyst after TPD under reflux in deionized water for 24 h. The water extracts were filtered and the presence of nickel halide in the supernatant liquids was determined by UV spectrophotometry using a Hitachi UV detector (model L-4700) equipped with a flow cell while the halide content was again measured using the Autotitrys technique as above.

The nature of any coke deposition was examined by temperature-programmed oxidation (TPO). A 100-mg sample of a demineralized, deactivated catalyst was ramped (10 K min^{-1}) to 1248 K in a 5% vol/vol O_2/He mixture. The effluent stream was analyzed by online TCD and the catalyst bed temperature was again independently monitored by the Pico data logger. An activated carbon (Darco G-60) and a graphite sample (synthetic 1- to 2-μm powder) supplied by Aldrich Chemicals, and demineralized in dilute mineral acid, were employed as model carbon materials in the TPO studies.

RESULTS AND DISCUSSION

Hydrodehalogenation of CB and BB: Single-Component Feedstock

The Ni/SiO_2 catalysts promoted solely hydrodechlorination (HDCl) and/or hydrodebromination (HDBr) reactions with no detectable cyclohexene, cyclohexane, or cyclohexyl chloride/bromide in the product stream. In contrast, Pd- and Rh-based catalysts have been reported to generate benzene and cyclohexane as hydrodechlorination products (30, 31). A loss of catalytic activity has been reported for hydrodehalogenation over an array of supported and unsupported transition metals catalysts (12, 16, 17, 21, 30, 32–34). The variation of the fractional conversion of both CB and BB (under identical reaction conditions) with time-on-stream over a representative catalyst is shown in Figs. 1a and 1b for short reaction periods. It can be seen that fractional conversions (x) of both CB and BB were essentially time invariant (Fig. 1a) and a resumption of the reaction after an overnight isothermal (673 K) treatment in flowing hydrogen delivered essentially superimposable time-on-stream profiles (Fig. 1b). Repeated and extended catalyst use was, however, accompanied by a gradual loss of activity. This effect is illustrated in Fig. 1c, wherein the ratio

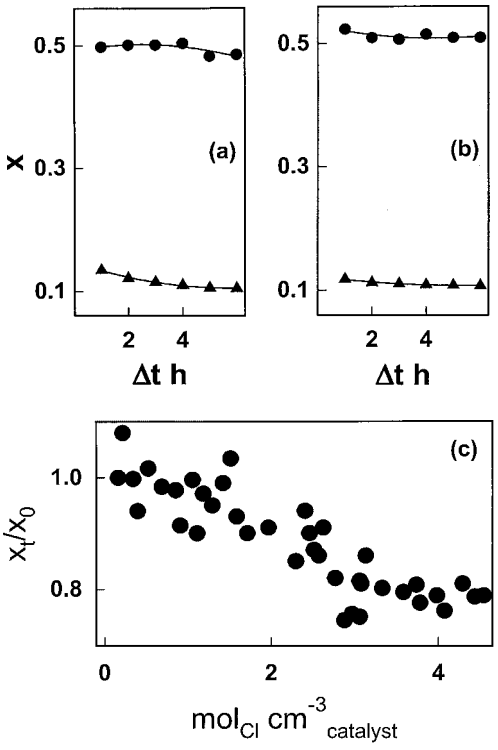

FIG. 1. Fractional conversion (x) of CB (●) and BB (▲) over a freshly activated (a) and used (b) 6.2% wt/wt Ni/SiO_2: $T = 573$ K, $W/F_{in} = 85\ g\ h^{-1}\ mol^{-1}$. (c) Ratio of time-dependent (x_t) to initial (x_0) fractional conversion of CB over 15.2% wt/wt Ni/SiO_2 at 573 K as a function of the concentration of chlorine that had been hydroprocessed.

of time-dependent to initial (x_t/x_0) fractional conversion is plotted as a function of the total concentration of Cl that had been hydroprocessed. The latter data were obtained from periodic sampling of the effluent stream for up to 800 h of continual operation, which corresponds to a total Cl/Ni mol ratio of 2×10^3. It should be noted that all catalytic data quoted in this paper represent steady-state activity where any long-term catalyst deactivation was negligible. The fractional conversion of BB was appreciably lower and temperatures up to 120 K higher than that employed in conversion of CB were necessary to attain comparable dehalogenation rates. It has been proposed (11, 35) that catalytic hydrodehalogenation involves the electrophilic attack of hydrogen on the adsorbed haloaromatic. Implicit in such a mechanism is the presumption that the aromatic ring in the transition state is cationic with respect to the initial state and electropositive substituents lower the activation barrier by stabilizing the transition state. The lower conversions of BB relative to CB are suggestive of a poorer activation of the C–Br bond for attack by hydrogen. This may be explained on the basis of the lower electron affinity of Br compared with that of Cl (36, 37), which translates into a less effective interaction with the catalyst surface.

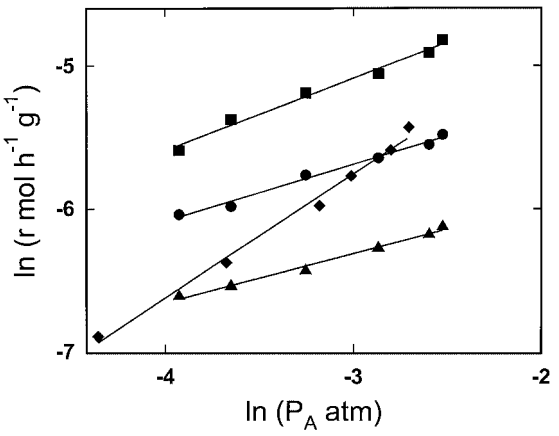

FIG. 2. Variation of HDCl rate with CB partial pressure at 473 (▲), 493 (●), and 523 (■) K and HDBr rate with BB partial pressure at 593 K (◆): $P_{H_2} = 0.9$ atm; 15.2% wt/wt Ni.

The dependence of the HDCl and HDBr rates on the partial pressures of the respective haloarenes is shown in Fig. 2. Given the lower reactivity of BB, a more limited database of meaningful HDBr kinetics is provided. The computed reaction orders indicate a fractional dependence on haloarene partial pressure that increased in magnitude with increasing temperature, i.e., 0.3 to 0.6 where $473\ K \leq T \leq 523$ K. The low partial order at 473 K is consistent with a high surface coverage by the reactant and the shift to greater dependencies with elevated temperature is suggestive of a temperature-induced desorption. The response of hydrodehalogenation rate to changes in the partial pressure of hydrogen is shown in Fig. 3, where, in contrast to the aromatic dependence, an increase in temperature lowered significantly the reaction order in hydrogen, from 0.7 (493 K) to 0.3 (553 K). Coq *et al.* (30) have reported an order close to 0.5 at low partial pressures of CB that they took to be

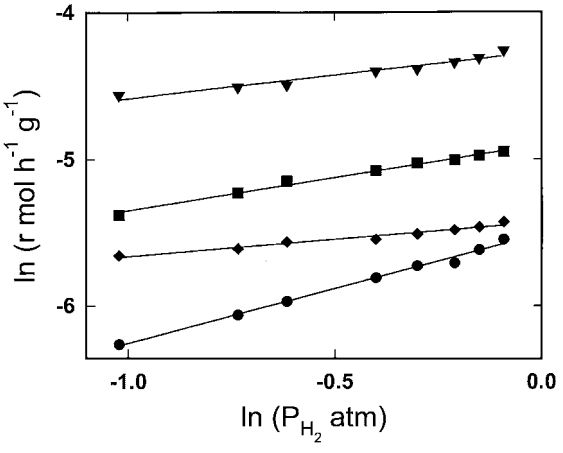

FIG. 3. Variation of HDCl rate with hydrogen partial pressure at 493 (●), 523 (■) and 553 (▼) K and HDBr rate with BB partial pressure at 593 K (◆): $P_{CB} = P_{BB} = 0.07$ atm; 15.2% wt/wt Ni.

indicative of a surface dissociation of hydrogen. Indeed, a number of workers have identified dissociated hydrogen as the reactive hydrogenolytic agent (12, 31, 38) and spillover hydrogen has also been proposed (32, 39) as the reactive species. In terms of an electrophilic mechanism there is ample evidence to support the existence of a reactive charged spillover hydrogen species (40). The decrease in reaction order with increasing temperature is suggestive of a catalytically significant hydrogen activation that is endothermic. The latter can be envisaged for spillover species where the dissociative energy of hydrogen is greater than the heat released during spillover onto the support or metal/support interface.

Effect of Hydrodehalogenation on Catalyst Structure

In every instance, the supported-metal size distribution was shifted to higher values after extended catalyst use, as illustrated by the TEM-derived histograms shown in Fig. 4. The used catalyst samples had each reached a stage of deactivation where the dehalogenation rate dropped by ca. 50% of the initial value. Gampine and Eyman (21) also noted an induced growth of Pd (on TiO_2, SiO_2, ZrO_2, and Al_2O_3) during a series of hydrodechlorination reactions. The Ni catalysts used in this study were prepared by deposition–precipitation, a synthesis route that is known (23, 41–44) to lead to strong metal/support interaction(s) with a high resistance to sintering. The freshly reduced sample (see Fig. 4) is characterized by a narrow distribution of Ni particle sizes, where the surface weighted average diameter (2.4 nm) is in good agreement with a recent independent report (41). The size distributions are much broader for the used samples; the average Ni particle size (9.9 nm) in the sample used to convert CB was greater than that (6.8 nm) associated with the spent catalyst from the BB reaction. A halide-induced agglomeration of Ni particles (on activated carbon) has been reported by Ohtsuka (20), who attributed this effect to a surface mobility of Ni–Cl species. Moreover, larger Ni crystallites are invariably generated from halide precursors due to a relatively facile crystallite growth of volatile $NiCl_2$. Vaporization of $NiCl_2$ crystals at temperatures as low as 573 K has been proposed to occur, leading to a deposition and growth of surface Ni particles (44). Chemical analysis of the activated catalysts before and after use did not reveal any significant loss of Ni from the spent samples.

It is clear that hydrodehalogenation has led to a restructuring of the Ni/SiO_2 and that the restructured catalysts delivered lower reaction rates. Hydrodehalogenation deactivation has been linked to a poisoning or site-blocking effect by the hydrogen halide that is produced (12, 17, 21, 33, 39) and halogens are known to act as electron acceptors with respect to supported transition metal systems (30, 31, 45). Carbon monoxide chemisorption has been used to good effect as a means of characterizing Ni/SiO_2 (46–50). The amounts of CO adsorbed on freshly activated and used catalysts are recorded in Table 1, where, with extended catalyst

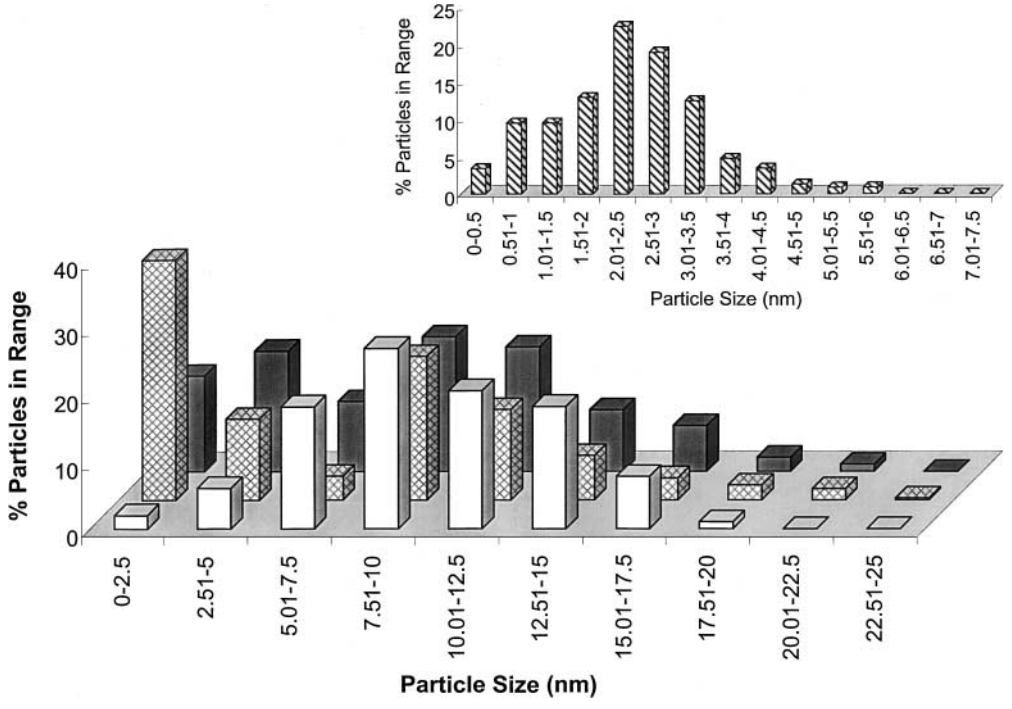

FIG. 4. Particle size distribution profiles of freshly reduced 11.9% wt/wt Ni/SiO_2 (hatched bars) and the same catalyst after extended use in the hydrodehalogenation of CB (open bars), BB (crosshatched bars), and 4-CBB (solid bars).

TABLE 1

CO Uptake (at 298 K) for Freshly Activated, Pretreated, and Used 15.2% wt/wt Ni/SiO_2 Catalysts

Pretreatment/reaction	CO adsorbed (μmol g_{Ni}^{-1})
Freshly activated	96
After prolonged use in CB hydrodechlorination at 548 K[a]	34
After prolonged use in BB hydrodebromination at 573 K[a]	16
After prolonged use in 4-CBB hydrodehalogenation at 573 K[a]	10
After direct contact with HCl	6
After direct contact with HBr	4

[a] Hydrodehalogenation activity had dropped to 50% of the initial value.

use, CO uptake was significantly reduced. It is known that CO chemisorption on supported metal catalysts is a function of the support, metal loading, temperature, and pressure (51, 52). Nevertheless, our observed decrease can be attributed, at least in part, to the formation of larger Ni crystallites during catalysis; the possibility of site blocking by residual surface halogen cannot be discounted. Temperature-programmed desorption (TPD) of CO can, however, shed some light on changes in the electronic properties of supported metal particles (46, 53, 54); the CO TPD profiles for the freshly activated catalysts are presented in Fig. 5. Each desorption profile is essentially featureless at $T < 773$ K and each is characterized by a main desorption peak ($T_{max} = 860$–920 K); a secondary shoulder at the higher temperature end of the principal peak was observed for the higher loaded samples. A direct comparison of the CO TPD profiles generated in this study with the limited published reports relating to Ni catalysts is problematic given the differences in metal loading/support/catalyst preparation/desorption procedure. CO desorption from Ni(110) generated a principal TPD peak at 400 K (55) whereas both high (>673 K)- and low (<473 K)-temperature CO desorption has been reported for Ni/MgO (47, 53), euro-Ni (56), and Ni/activated carbon (57). The consensus of opinion is that a higher desorption temperature is characteristic of dissociatively adsorbed CO (47, 57). The TPD profiles for each Ni/SiO_2 suffered a marked disruption after catalyst use, as shown in Fig. 6, taking the 15.2% wt/wt Ni/SiO_2 as representative. The desorption peaks were broadened, and in the case of the catalyst used to convert CB, the T_{max} for the main peak was shifted upward by up to 30 K. Extended use in hydrodebromination generated two desorption peaks, a shift of the principal T_{max} to 1085 K and a secondary peak at 900 K. This behavior is indicative of an overall stronger interaction with CO and is diagnostic of an appreciable electronic perturbation of the Ni crystallites. Doping Ni/SiO_2 with alkali adatoms has been shown to disrupt CO adsorption through electron enrichment of the metal phase (58). Arena *et al.* concluded that alkali metal dopants weaken CO/Ni interactions (53, 59). As a corollary to the latter, electron withdrawal due to halogen/catalyst interaction(s) must serve to strengthen the CO–Ni bonding with a consequent shift in CO TPD to higher temperatures. Moreover, the desorption of CB from a freshly activated 6.2% wt/wt Ni/SiO_2 catalyst took place in a single step at ca. 800 K whereas a continuous desorption of CB occurred for the deactivated sample at $T > 810$ K. As with CO adsorption, CB was more strongly held on the deactivated surface, which may also account to some extent for the lower conversions.

We have shown elsewhere (24) that the catalyst surface, under reaction conditions, is saturated with hydrogen halide. Moreover, STEM/EDX elemental maps of the used catalysts revealed an appreciable halogen concentration on the surface (60). We determined the reversibly and irreversibly held halogen component on the used catalysts by a potentiometric methodology (see Experimental). Analysis by UV spectrophotometry of the aqueous extracts from a refluxing of the spent samples yielded spectra that are characteristic (peak at 395–400 nm) of nickel halide, as shown for a representative Ni/SiO_2 in Fig. 7, which also includes spectra for both the aqueous extract of the freshly activated

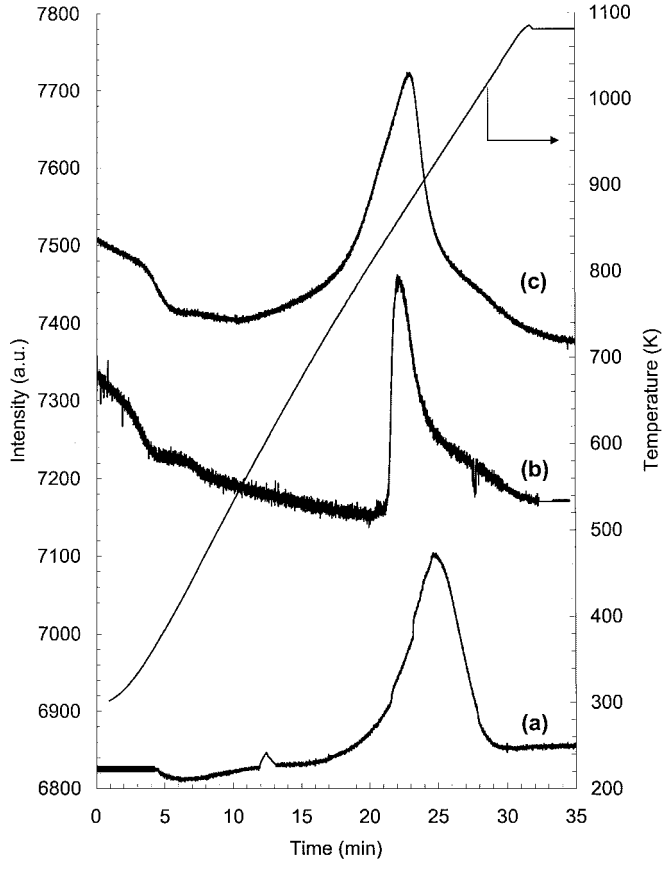

FIG. 5. CO TPD profiles for the freshly activated 6.2 (a), 11.9 (b), and 15.2% (c) wt/wt Ni/SiO_2.

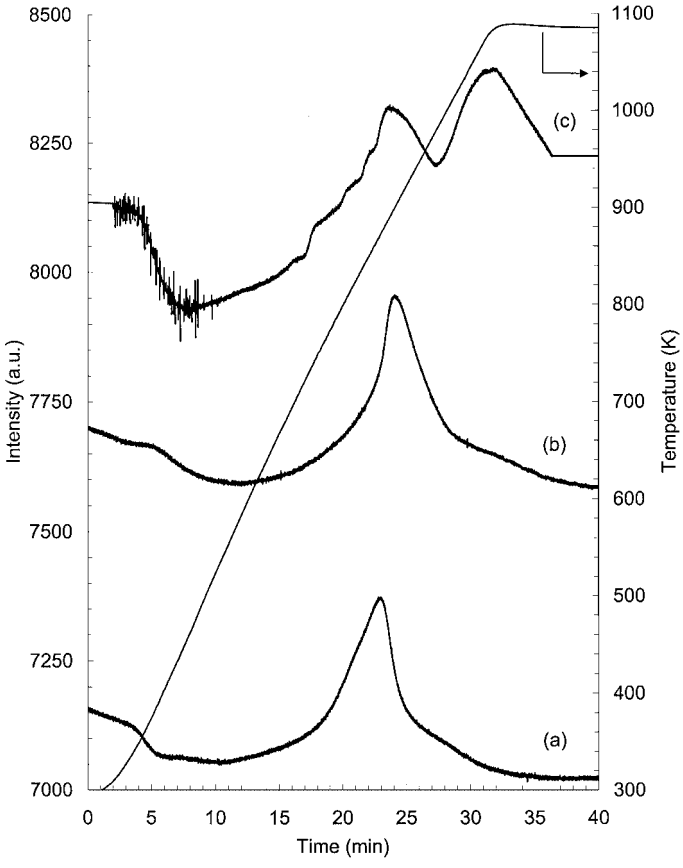

FIG. 6. CO TPD profiles (a) for freshly activated 15.2% wt/wt Ni/SiO_2, and for the same sample after (b) extended use in the HDCl of CB and (c) extended use in the HDBr of BB.

Ni/SiO_2 (blank) and $NiCl_2$ (0.01 mol dm^{-3}) for comparative purposes. The latter provides indirect evidence that the surface halide is built into the Ni sites. It should be noted that the solid, prior to reflux, had undergone a prolonged thermal desorption treatment in H_2, which has been shown to be effective in removing surface HCl (24); hydrolysis of residual HCl during reflux with subsequent reaction to form $NiCl_2$ can be discounted. The coexistence of reversibly and irreversibly bound Cl on the catalyst surface during hydrodechlorination has been established elsewhere (12, 24, 30). Potentiometric determination of our scrubbing solution (containing the reversibly held halogen) and refluxed water extract (containing the irreversibly held halogen) yielded the results provided in Table 2. A subsequent elemental mapping of the refluxed solid did not reveal even trace quantities of halogen on the surface; i.e., the combined thermal desorption (in H_2) and reflux treatment was fully effective in extracting the entire halogen component from the spent catalysts. The residual halogen content after hydroprocessing the CB feed was appreciably higher than that remaining after the BB reaction, in keeping with the overall higher HDCl rates. There was a considerable irreversibly held halogen component in these catalysts that was greater in the case of Br. The latter finds some support in the work of Yu *et al.* (17), who attributed a stronger "poisoning effect" to HBr compared with HCl but did not identify the reason for this effect. The presence of a "built-in" surface halogen has been shown to result in strong electronic

TABLE 2

Potentiometric Analysis of the Halogen Content after Thermal Desorption (Reversible) and Extraction (Irreversible) from 11.9% wt/wt Ni/SiO_2 after a Number of Hydrodehalogenation Reactions

Feedstock	Total Cl/Ni	Total Br/Ni	Reversibly held halogen (%)	Irreversibly held halogen (%)
CB	0.11	—	63	37
BB	—	0.040	22	78
CB + BB[a]	0[b]	0.045	38	62
2-CBB	0[b]	0.076	45	55

Note. $T = 603$ K. Total feed hydroprocessed, 5.8×10^{-3} mol.
[a] Equimolar mixture.
[b] No detectable Cl.

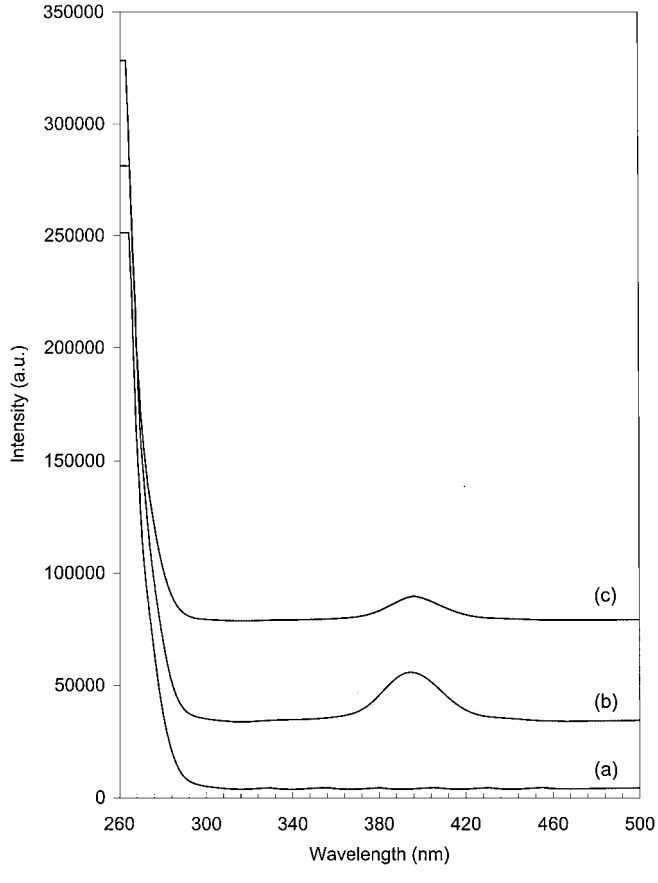

FIG. 7. UV spectra of (a) the liquid extract after reflux treatment of a freshly activated 15.2% wt/wt Ni/SiO_2 catalyst, (b) a $NiCl_2$ (0.01 mol dm^{-3}) aqueous solution, and (c) the liquid extract after reflux treatment of a CB-deactivated 15.2% wt/wt Ni/SiO_2 catalyst.

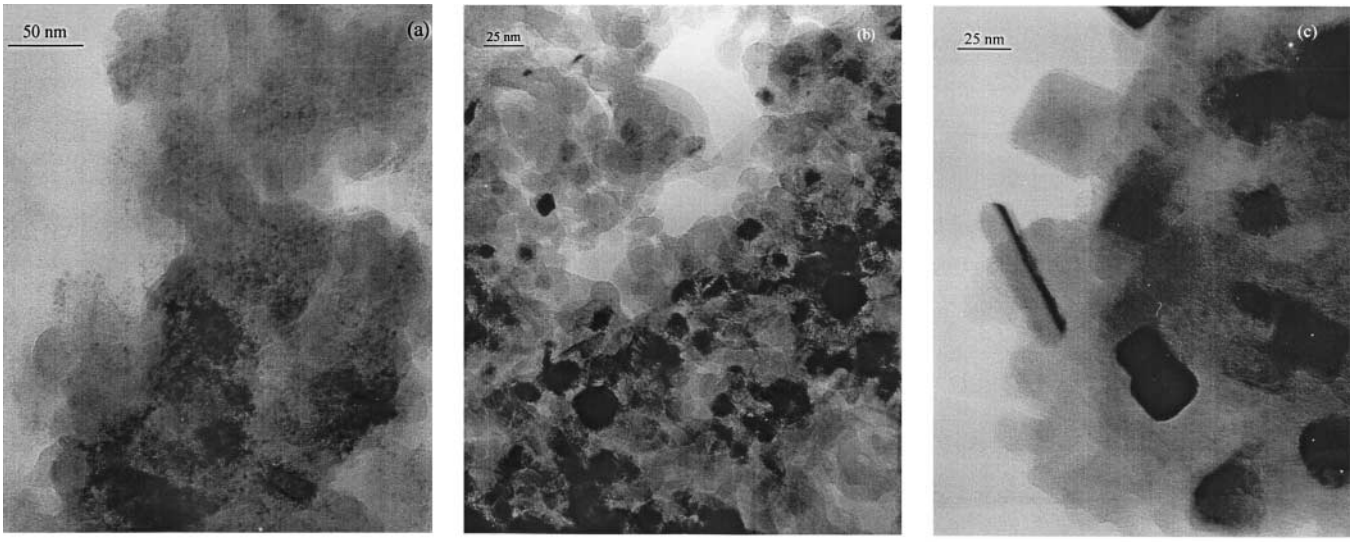

FIG. 8. TEM micrographs illustrating the morphology of the nickel crystallites (a) on freshly activated 15.2% wt/wt Ni/SiO_2, and on the same catalyst after (b) extended use in the HDBr of BB and (c) direct contact with HCl.

perturbations of the Ni sites, leading to a disruption to the hydrogen dissociation step (39, 44) and a consequent loss of hydrogenolysis activity. In terms of CO TPD behavior (Fig. 6), the appearance of two high-temperature desorption peaks from the HDBr catalyst is diagnostic of both a very strong CO interaction and a significant modification of the Ni sites. It has been shown in single-crystal studies that any reconstruction of the Ni surface that causes a lengthening of the Ni–Ni bonds results in a deeper penetration by adsorbates (61). Given the appreciable halogen (particularly Br) component that appears to be built into the Ni sites (Table 2), this must induce some restructuring, where the bulkier Br will induce greater change in the lattice structure, leading to stronger CO adsorption. We tentatively attribute the observed variance in CO TPD from the spent HDBr and HDCl catalysts to this effect. Metal site restructuring, notably particle growth, after catalysis is well illustrated by the representative TEM micrographs included in Fig. 8, wherein the presence of larger faceted Ni particles in the spent sample is evident. A direct contact of the freshly activated catalyst with HCl and/or HBr resulted in an even greater modification of the supported metal phase. Such a direct interaction with the hydrogen halide is more extreme than that which results during hydrodehalogenation and the changes that are wrought to catalyst morphology are accordingly greater. Indeed, the hydrogen halide treatment resulted in a complete change in Ni particle morphology and an array of particle sizes and geometrical shapes are evident in the TEM micrograph (Fig. 8c) that was not observed for the spent catalysts.

The nature of carbon laydown in the spent catalysts was probed by means of temperature-programmed oxidation (TPO), where the original Ni metal content was removed from the samples by a demineralization treatment to ensure that gasification of carbon was not catalyzed by any residual Ni. A TPO profile for a representative used catalyst is shown in Fig. 9, which also includes profiles generated for model amorphous and graphitic carbon samples. It is well established (62) that an increasing order in carbon structure, i.e., a move from an amorphous to a graphitic nature, is accompanied by an increase in the temperature at which gasification is initiated and this is indeed borne out in Fig. 9. The catalytically generated carbon is essentially amorphous with a negligible ordered component. An appreciable amorphous carbon content (up to 8% wt/wt) was recorded for the used samples. The presence of residual Cl on a catalyst surface has been noted elsewhere to result in a greater degree of coke formation (63–65). A displacement of charge density from the surface nickel sites can also occur through the carbon deposits on the catalyst, where such deposits retain a halogenated character. The observed loss of activity can be linked to a less effective activation of the aromatic or hydrogen reactants and/or a blocking of active sites by carbonaceous deposits. Work is now ongoing to characterize the composition/nature of the coke that is formed during hydrodehalogenation.

Hydrodehalogenation of CB and BB: Mixed-Component Feedstock

Given the appreciably higher reactivity of CB compared with BB in the single-component systems, it is to be expected that HDCl should far exceed HDBr in a mixed reactant feedstock. Hydrodehalogenation was again the only catalyzed reaction and there was no evidence of any ring reduction. Selected catalytic data for the conversion of mixed

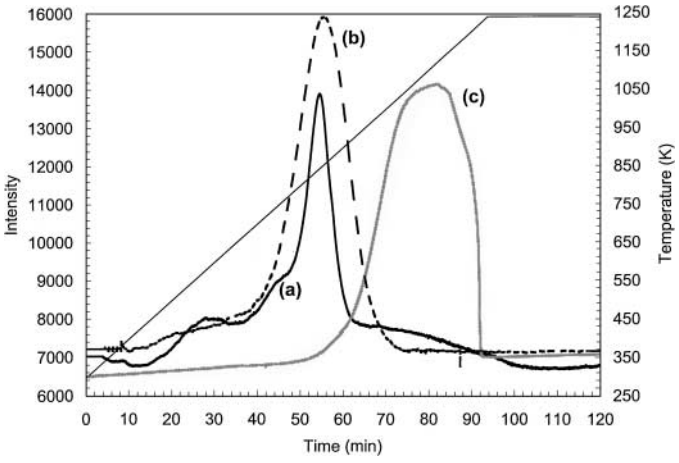

FIG. 9. TPO profiles generated from (a) a sample of 15.2% wt/wt Ni/SiO_2 after extended use in the HDCl of CB (solid line), (b) amorphous carbon (dashed line), and (c) graphitic carbon (dotted line).

CB/BB feed are given in Table 3, where the total inlet haloaromatic feed rate was kept constant. The haloarenes were fed to the reactor in methanol or hexane (prior to vaporization) in order to achieve comparable and meaningful W/F_{in}; the gas-phase dehalogenation rate and product composition were largely unaffected by the nature of the solvent (polarity). Based on an analysis of the product stream, it appears that the presence of BB in the feed had a severely limiting effect on the fractional conversion of CB. Under the same reaction conditions, the degree of dechlorination of a solely CB feed was appreciably greater while the HDBr rates for a single-component BB (at the same inlet molar feed rates) were lower by a factor of up to 5 than those given in Table 3.

This apparent decline in HDCl due to the presence of BB in the feed was probed by considering the reactivity of single- and dual-component permutations from a choice of CB, BB, benzene, HCl, and HBr as reactants. The inlet molar feed rate of each haloarene was kept constant and the fractional conversions of CB and BB are given in Table 4. Once again, the overall degree of CB dechlorination (based on product composition) was inhibited in the presence of BB while in the inclusion of CB in the feed raised the degree of debromination. Passage of a mixture of BB and HCl over the catalyst resulted in CB formation but there was no evidence of any BB in the product stream from a mixed CB/HBr feed. The former result can be attributed to a surface chlorination of the benzene that is formed from the HDBr of BB; any surface HBr does not participate in an analogous bromination. Moreover, the degree of dechlorination was also suppressed in the presence of benzene, an effect that was not observed in the case of BB/benzene. There was no evidence of any formation of chlorobromobenzene (CBB), which indicates that any HCl or HBr that was generated via HDCl or HDBr steps, respectively, did not then react with the incoming haloaromatic reactant. The latter is to be expected on the basis of the deactivating effect of the halogen substituent (66). Moreover, passage of benzene in the presence of HCl or HBr did not result in any measurable CB or BB in the effluent stream. The generation of CB from either a BB/HCl or BB/CB mix must be the result of a concerted attack of surface HCl on the adsorbed aromatic carbonium ion intermediate. Hydrodechlorination of the more reactive CB, in effect, chlorinates the catalyst surface, as discussed elsewhere (67). The observed decrease in CB conversion in the mixed CB/BB feed is the result of what amounts to an exchange reaction, where the debrominated intermediate is subsequently chlorinated by surface HCl. Potentiometric analysis of spent catalyst samples from the treatment of BB/CB mixtures did not reveal any measurable quantities of residual chlorine (see Table 2), presumably due to the reactivity of this surface HCl. In the mixed CB/BB feed, the surface reactions involve cycles of HDCl/HDBr. The presence of CB or HCl in the BB feed served to raise the degree of debromination due to a combined HDBr and

TABLE 3

Inlet (in) and Outlet (out) Cl/Br Molar Ratios, Fractional Conversion of CB (x_{Cl}), and BB (x_{Br}) and Overall Hydrodehalogenation Rate (r) for the Conversion of Mixed CB/BB Feed in Methanol and *n*-Hexane over 15.2% wt/wt Ni/SiO_2

Solvent	$[Cl]_{in}/[Br]_{in}$	$[Cl]_{out}/[Br]_{out}$	x_{Cl}	x_{Br}	$10^4\, r$ (mol h^{-1} g_{Ni}^{-1})
n-Hexane	3.0	2.5	0.23	0.07	4.3
Methanol	3.0	2.9	0.22	0.12	4.2
n-Hexane	2.0	3.0	0.05	0.51	4.1
n-Hexane	1.0	1.9	0.04	0.50	3.8
n-Hexane	0.5	1.4	0.03	0.52	3.6
n-Hexane	0.3	0.6	0.05	0.52	3.1
Methanol	0.3	0.7	0.04	0.50	2.9

Note. $T = 573$ K. $W/F_{in} = 3125$ g mol^{-1} h^{-1}.

TABLE 4

Fractional Conversion of CB (x_{Cl}) and BB (x_{Br}) in an Array of Single and Dual-Reactant Mixtures[a]

Feedstock	x_{Cl}	x_{Br}
CB	0.65	—
BB	—	0.73
CB + BB	0.02	0.90
CB + benzene	0.30	—
BB + benzene	—	0.75
CB + HBr	0.54	—
BB + HCl	—[b]	0.82

[a] 11.9% wt/wt Ni/SiO_2; $F_{Cl} + F_{Br} = 1.7 \times 10^{-4}$ mol h^{-1}; $[Cl_{in}]/[Br_{in}] = 3$; $T = 573$ K.
[b] $[CB_{out}]/[BB_{out}] = 0.07$.

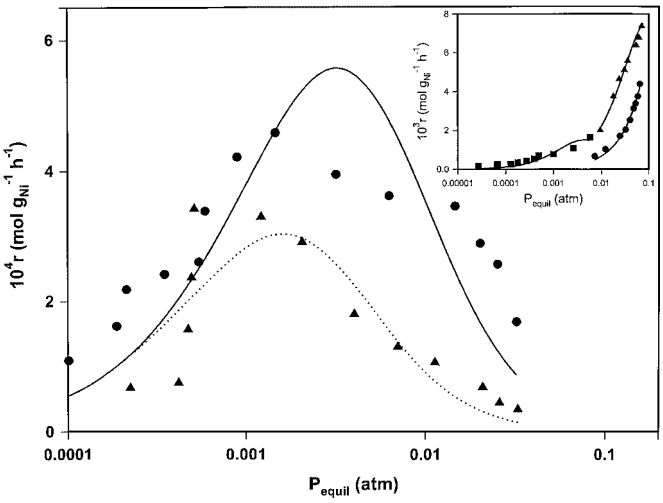

FIG. 10. Hydrodehalogenation rate (r) over 15.2% wt/wt Ni/SiO_2 as a function of the equilibrium partial pressure of 2-CBB (▲, dotted line) and 3-CBB (●, solid line): solvent, *n*-hexane; $T = 553$ K; $P_{H_2} = 0.90$ atm. (Inset) Rates of hydrodehalogenation of 4-CBB (■, 553 K), HDCl of CB (▲, 523 K), and HDBr of BB (●, 593 K) as a function of the haloarene equilibrium partial pressure. Note: The lines represent Model B predictions.

hydrochlorination (Cl exchange) as composite steps in the removal of Br from the aromatic host.

Hydrodehalogenation of CBB Isomers: Single-Component Feedstock

Contacting each catalyst with the CBB isomers during reaction also resulted in an increase in Ni particle size; see the representative histogram given in Fig. 4, where the average surface weighted particle diameter equals 8.3 nm. The variation of the hydrodehalogenation rate of the three CBB reactants as a function of the equilibrium haloarene partial pressure at a fixed temperature (553 K) is shown in Fig. 10. The rate/pressure dependencies for the hydrodehalogenation of CB and BB under comparable reaction conditions are presented in the inset to Fig. 10. The presence of the second halogen substituent severely lowered the reaction rates, again in keeping with an electrophilic mechanism, where the additional electron withdrawing substituent has a deactivating effect. Dehalogenation rates follow the sequence 4-CBB > 3-CBB > 2-CBB, which is strongly suggestive of steric hindrance limitations that serve to further lower the extent of hydrodehalogenation and outweigh any contribution due to positional inductive effects. Similar behavior has also been reported for the gas-phase hydrodechlorination of trichlorophenols (68), where steric rather than resonance considerations governed reactivity. The rate vs partial pressure profiles pass through a maximum in the case of 2-CBB and 3-CBB but increased continuously in the case of 4-CBB over the range of pressures that were considered; the maximum inlet pressure in the latter case was limited by the solubility of 4-CBB in *n*-hexane. Dehalogenation of CB and BB likewise exhibited a continuous increase.

The published haloarene HDCl kinetic studies have largely been based on pseudo-first-order approximations (10, 69, 70) and there have been few attempts to construct kinetic models from mechanistic considerations (28, 36, 71–73). The appearance of maxima, indicating rate inhibition at higher pressures, is characteristic of a system that adheres to a Langmuir–Hinshelwood-type mechanism. Under the reaction conditions employed in this study, hydrodehalogenation has been shown to be irreversible (24) and the surface reaction can be taken to be rate limiting. Seven Langmuir–Hinshelwood-type kinetic approximations present themselves (74).

Model A—Both hydrogen and haloarene adsorb associatively, competing for the same surface sites with no product inhibition.

Model B—The haloarene adsorbs associatively and hydrogen adsorbs dissociatively, with simultaneous reaction on the same sites and no product inhibition.

Model C—The haloarene adsorbs associatively and hydrogen adsorbs dissociatively on different sites with no product inhibition.

Model D—This is the same as Model A but with noncompetitive adsorption.

Model E—This is the same as Model C but with the addition of the first hydrogen atom being the slow step and the second hydrogen atom reacting in a much faster step.

Model F—This is the same as Model C but with strong HCl or HBr adsorption.

Model G—This is the same as Model D but with strong HCl or HBr adsorption.

The mathematical expressions associated with each model are presented as a footnote in Table 5; the applicability of each model can be assessed from the table entries. Adopting the discrimination criteria outlined under Experimental (minimum values of both the sum of residual squares (χ^2) and the average relative percentage error (ε) and application of the F-test) the best fits were obtained with Models A, B, C, and E. Only Models A and B, however, were capable of reproducing the rate maxima observed in the case of 2-CBB and 3-CBB. Given the evidence, discussed above, that supports the involvement of dissociated hydrogen, Model B rests on a more solid mechanistic basis. The kinetic and adsorption constants extracted from the Model B treatment of the experimental data presented in Fig. 10 are listed in Table 6. While this model proved adequate in reproducing the experimental rate/pressure profiles for single-component reaction systems, an attempt to simulate the hydrodehalogenation of both CB and BB in a mixed feed (Fig. 11) failed. The simulation was made by including the adsorption term for each haloarene, obtained from the fit to the single-component reaction systems, to generate a composite term. The estimated dehalogenation rates of CB and BB are significantly higher

TABLE 5

Tests of Statistical Significance for the Different Kinetic Models Applied to the Experimental Data Presented in Fig. 10[a]

	Model A			Model B			Model C			Model D			Model E			Model F			Model G		
Reactant	F_C/F	ε (%)	$\chi^2 \times 10^8$	F_C/F	ε (%)	$\chi^2 \times 10^8$	F_C/F	ε (%)	$\chi^2 \times 10^8$	F_C/F	ε (%)	$\chi^2 \times 10^8$	F_C/F	ε (%)	$\chi^2 \times 10^8$	F_C/F	ε (%)	$\chi^2 \times 10^8$	F_C/F	ε (%)	$\chi^2 \times 10^8$
2-CBB	9.0	34.6	4.27	9.3	40.9	4.11	2.1	96.6	14.16	0	100.0	46.84	5.2	61.3	6.92	0	86.8	44.46	0	94.2	44.08
3-CBB	26.7	19.7	4.91	10.3	32.0	12.03	14.6	24.6	8.68	14.6	24.6	8.68	63.7	13.9	2.10	9.9	24.2	8.69	0.3	81.0	91.30
4-CBB	11.8	34.2	24.67	10.1	37.1	28.55	24.0	21.8	12.41	0	100.0	566.8	79.6	9.3	3.80	35.6	15.3	52.25	35.6	15.3	5.23
CB	185.3	4.1	68.41	167.4	4.1	75.71	234.7	4.3	54.06	234.7	4.3	54.06	136.5	7.1	92.76	134.5	4.3	54.07	134.5	4.3	54.06
BB	195.1	7.8	14.88	195.2	7.8	14.89	195.2	7.8	14.88	195.2	7.8	14.88	195.2	7.8	14.88	111.2	7.6	14.93	111.4	7.7	14.90

[a] Mathematical expressions for each model. A: $r = \frac{kK_AK_HP_AP_{H_2}}{(1+K_AP_A+K_HP_{H_2})^2}$; B: $r = \frac{kK_AK_HP_AP_{H_2}}{(1+K_AP_A+\sqrt{K_HP_{H_2}})^3}$; C: $r = \frac{kK_AK_HP_AP_{H_2}}{(1+K_AP_A)(1+\sqrt{K_HP_{H_2}})^2}$; D: $r = \frac{kK_AK_HP_AP_{H_2}}{(1+K_AP_A)(1+K_HP_{H_2})}$; E: $r = \frac{kK_AK_H\sqrt{P_AP_{H_2}}}{(1+K_AP_A)(1+\sqrt{K_HP_{H_2}})}$;
F: $r = \frac{kK_AK_HP_AP_{H_2}}{(1+K_AP_A+K_{HX}P_{HX})(1+\sqrt{K_HP_{H_2}})^2}$; G: $r = \frac{kK_AK_HP_AP_{H_2}}{(1+K_AP_A+K_{HX}P_{HX})(1+K_HP_{H_2})}$.

TABLE 6

Kinetic (k) and Adsorption (K) Constants Associated with Model B[a] Treatment of the Experimental Data Presented in Fig. 10

Reactant	k (mol g_{Ni}^{-1} h^{-1})	K_A (atm^{-1})	K_H (atm^{-1})
2-CBB	0.4	330	0.005
3-CBB	0.5	170	0.01
4-CBB	0.6	130	0.03
CB	0.7	7	0.2
BB	0.8	0.7	3

[a] Model B: $r = \frac{kK_AK_HP_AP_{H_2}}{(1+K_AP_A+\sqrt{K_HP_{H_2}})^3}$.

and lower, respectively, than the experimental values. Moreover, discontinuities observed in the experimentally determined HDCl and HDBr rates are not captured by the model. This inability to reproduce reaction data for the dual-component system must be due to the contribution of hydrochlorination/Cl exchange to the overall process, an effect that cannot be taken into account in the mathematical modeling. A more detailed kinetic analysis, outside the scope of the present work, must be undertaken to establish a specific rate expression that incorporates a term for the exchange/surface chlorination step.

The relationship between benzene selectivity and the inlet CBB partial pressure is given in Fig. 12; in every instance the selectivity with which a full dehalogenation proceeded decreased with increasing partial pressure. The more reactive 4-CBB delivered appreciably higher selectivities in terms of complete dehalogenation. The higher values of $S_{benzene}$ from 2-CBB compared with 3-CBB can be attributed to geometric effects where the removal of both halogen substituents in adjacent positions on the ring (2-CBB) is more likely to occur than a concerted removal

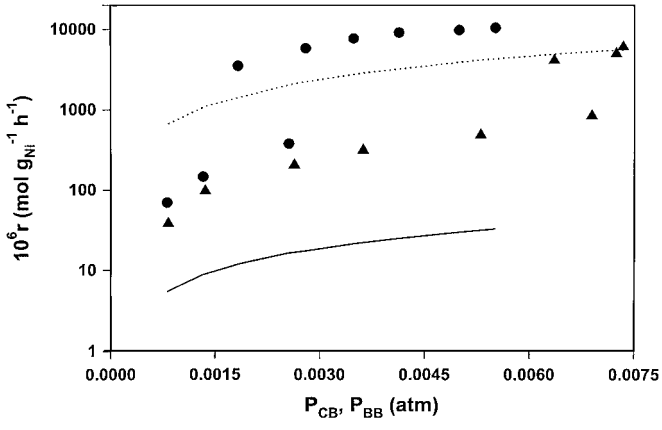

FIG. 11. Hydrodehalogenation rates (r) of CB and BB (mixed-component feedstock) over 15.2% wt/wt Ni/SiO_2 as a function of the equilibrium partial pressure of CB (▲) and BB (●): total haloarene partial pressure, 0.011 atm; solvent, n-hexane; $T = 573$ K; $P_{H_2} = 0.90$ atm. (Dotted and solid lines) Model B simulations for the hydrodehalogenation of CB and BB, respectively.

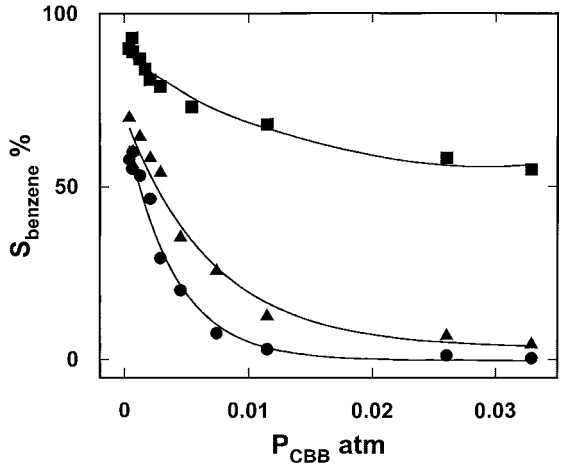

FIG. 12. Benzene selectivity from the hydrodehalogenation of 2-CBB (▲), 3-CBB (●), and 4-CBB (■) over 15.2% wt/wt Ni/SiO_2 as a function of the partial pressure of the haloaromatic: $T = 553$ K; $P_{H_2} = 0.96$ atm.

of the halogens in the *meta*-isomer (3-CBB). As in the case of the mixed CB/BB feedstock, debromination exceeded dechlorination. Moreover, an increase in temperature served to further shift the selectivity in favor of complete dehalogenation (see Table 7 for representative selectivity data). A similar temperature effect has been noted elsewhere for the dechlorination of polychlorinated aromatics (68). In common with the CB/BB mixtures, the catalyst samples used in the conversion of CBB (Table 2) did not contain any measurable residual chlorine, while there was appreciable bromine content.

TABLE 7

Effect of Temperature and Inlet Haloarene Partial Pressure on Product Selectivity for the Conversion of 2-CBB, 3-CBB, and 4-CBB over 15.2% wt/wt Ni/SiO_2, $P_{H_2} = 0.96$ atm

P (atm)	T (K)	S_{CB} (%)	S_{BB} (%)	$S_{benzene}$ (%)
2-CBB feed				
0.0004	553	30	0	70
0.0004	593	22	0	78
0.0029	553	46	0	54
0.0029	593	28	0	72
0.012	553	85	3	12
0.012	593	67	5	28
0.033	553	88	7	5
0.033	593	76	12	12
3-CBB feed				
0.0004	553	45	0	55
0.0004	593	34	0	66
0.0029	553	71	0	29
0.0029	593	51	0	49
0.012	553	96	1	3
0.012	593	89	2	9
0.033	553	98	1	<1
0.033	593	89	6	5
4-CBB feed				
0.0004	553	10	0	90
0.0004	593	8	<1	92
0.0029	553	21	0	79
0.0029	593	15	<1	85
0.012	553	32	0	68
0.012	593	24	2	74
0.033	553	45	0	55
0.033	593	27	3	70

CONCLUSIONS

The results presented in this paper support the following:

(i) Hydrodehalogenation of single-component CB or BB feed generates benzene as the sole product, leaving the aromatic ring intact in every instance where the dechlorination rate far exceeds debromination under the same reaction conditions.

(ii) The Ni/SiO_2 catalysts were subject to a long-term deactivation that can be linked to an electronic perturbation of the Ni crystallites caused by electron withdrawal due to halogen/catalyst interaction(s), possible site blocking by the halogen adatom, and deposition of amorphous carbon.

(iii) The spent catalyst samples contain an appreciable halogen component, a significant alteration to the morphology of the Ni crystallites, and an overall increase in the average particle size, which can be attributed to the more facile agglomeration of surface nickel halides.

(iv) Hydrodehalogenation rate decreases in the order CB > BB > 4-CBB > 3-CBB > 2-CBB, which is consistent with an electrophilic mechanism where dehalogenation in the case of CBB is governed by steric considerations. The degree of debromination of a single CBB reactant and CB/BB mixtures is higher than that achieved in a single-component BB feed under comparable conditions as a result of the reactivity of surface HCl, which facilitates a hydrochlorination or Cl exchange with aromatic Br;

(v) The reaction orders with respect to CB, BB, and H_2 are temperature dependent. The experimentally determined rate/pressure profiles can be represented by a standard Langmuir–Hinshelwood model involving the associative adsorption of the haloarene and the dissociative desorption of hydrogen on the same catalyst sites with no product inhibition. This model is, however, unable to simulate hydrodehalogenation of CB/BB mixtures feed, as it does not take into account the additional Cl exchange reaction.

ACKNOWLEDGMENTS

This work was supported in part by a grant (GR/M51420) from the Engineering and Physical Sciences Research Council. The authors are grateful to Dr. R. Brydson for his assistance with the TEM analysis and to George Tavoularis for the provision of some hydrodehalogenation data. JLV acknowledges financial support from the Ministerio de Education y Cultura in Spain (Subprograma de intercambio temporal con la Royal Society de Londres).

REFERENCES

1. Moriarty, F., "Organochlorine Insecticides: Persistent Organic Pollutants." Academic Press, London, 1975.
2. Howe-Grant, M., Ed., "Kirk-Othmer Encyclopedia of Chemical Technology," 4th Ed., Vol. 1. Wiley, New York, 1991.
3. Forni, P., Prati, L., and Rossi, M., *Appl. Catal. B* **14**, 49 (1997).
4. Perrone, L., Prati, L., and Rossi, M., *Appl. Catal. B* **15**, 241 (1998).
5. Murena, F., Famiglietti, V., and Gioia, F., *Environ. Prog.* **12**, 231 (1995).
6. Creyghton, E. J., Burgers, M. H. W., Jansen, J. C., and van Bekkum, H., *Appl. Catal. A* **128**, 275 (1995).
7. Srinivas, S. T., Lakshmi, L. J., Lingaiah, N., Prasad, P. S. S., and Rao, P. K., *Appl. Catal. A* **135**, 1201 (1996).
8. Srinivas, S. T., Prasad, P. S. S., and Rao, P. K., *Catal. Lett.* **50**, 77 (1998).
9. Srinivas, S. T., Prasad, P. S. S., Madhavendra, S. S., and Rao, P. K., *Stud. Surf. Sci. Catal.* **113**, 835 (1998).
10. Hagh, B. F., and Allen, D. T., *AIChE J.* **36**, 773 (1990).
11. Suzdorf, A. R., Morozov, S. V., Anshit, N. N., Tsiganova, S. I., and Anshit, A. G., *Catal. Lett.* **29**, 49 (1994).
12. Estelle, J., Ruz, J., Cesteros, Y., Fernandez, R., Salagre, P., Medina, F., and Sueiras, J. E., *J. Chem. Soc. Faraday Trans.* **92**, 2811 (1996).
13. Cesteros, Y., Salagre, P., Medina, F., and Sueiras, J. E., *Appl. Catal. B* **25**, 213 (2000).
14. Cesteros, Y., Salagre, P., Medina, F., Sueiras, J. E., Tichit, D., and Coq, B., *Appl. Catal. B* **32**, 25 (2001).
15. Wei, B., Li, S., Lee, H. K., and Hor, T. S. A., *J. Mol. Catal. A* **126**, 183 (1997).
16. Aramendia, M. A., Borau, V., Garcia, I. M., Jimenez, C., Marinas, J. M., and Urbano, J., *Appl. Catal. B* **20**, 101 (1999).
17. Yu, Z., Liao, S., and Xu, Y., *React. Funct. Polym.* **29**, 151 (1996).
18. Frankel, K. A., Jang, B. W. L., Roberts, G. W., and Spivey, J. J., *Stud. Surf. Sci. Catal.* **111**, 239 (1997).
19. Windaw, M., and Zhang, D. P., *Catal. Today* **30**, 99 (1996).
20. Ohtsuka, Y., *J. Mol. Catal.* **54**, 225 (1989).
21. Gampine, A., and Eyman, D. P., *J. Catal.* **170**, 315 (1998).
22. Zhuang, S., Wu, J., Liu, X., Tu, J., Ji, M., and Wandelt, K., *Surf. Sci.* **331**, 42 (1995).
23. Keane, M. A., *Can. J. Chem.* **72**, 372 (1994).
24. Tavoularis, G., and Keane, M. A., *J. Chem. Technol. Biotechnol.* **74**, 60 (1999).
25. Ruthven, D. M., *Chem. Eng. Sci.* **23**, 759 (1968).
26. Mears, D. E., *Ind. Eng. Proc. Des. Dev.* **10**, 453 (1971).
27. Valverde, J. L., Zumalacarregui, L., de Lucas, A., and Suris, G., *AIChE J.* **43**, 2141 (1997).
28. Valverde, J. L., Zumalacarregui, L., de Lucas, A., and Suris, G., *Trans. Inst. Chem. Eng.* **75**, 78 (1997).
29. Valverde, J. L., de Lucas, A., and Rodriguez, J. F., *Ind. Eng. Chem. Res.* **38**, 251 (1999).
30. Coq, B., Ferrat, G., and Figueras, F., *J. Catal.* **101**, 434 (1986).
31. Bodnariuk, P., Coq, B., Ferrat, G., and Figueras, F., *J. Catal.* **116**, 459 (1989).
32. Kovenklioglu, S., Cao, Z., Shah, D., Farrauto, R. J., and Balko, E. N., *AIChE J.* **38**, 1003 (1992).
33. Shin, E.-J., and Keane, M. A., *Appl. Catal. B* **18**, 241 (1998).
34. Bozzelli, J. W., Chen, Y. M., and Chuang, S. S. C., *Chem. Eng. Commun.* **115**, 1 (1992).
35. Shin, E.-J., and Keane, M. A., *Chem. Eng. Sci.* **54**, 1109 (1999).
36. Dean, J. A., "Handbook of Organic Chemistry." McGraw–Hill, New York, 1987.
37. Huang, H. Y., Yang, R. T., and Chen, N., *Langmuir* **15**, 7647 (1999).
38. Kraus, M., and Bazant, V., *in* "Proceedings, 5th International Congress on Catalysis, Palm Beach, 1972" (J. W. Hightower, Ed.), p. 1073. North Holland, Amsterdam, 1969.
39. Shin, E.-J., Spiller, A., Tavoularis, G., and Keane, M. A., *Phys. Chem. Chem. Phys.* **1**, 3173 (1999).
40. Roland, U., Braunschweig, Th., and Rossler, F., *J. Mol. Catal. A* **127**, 61 (1997).
41. Burattin, P., Che, M., and Louis, C., *J. Phys. Chem. B* **103**, 6171 (1999).
42. Richardson, J. T., and Dubus, R., *J. Catal.* **54**, 207 (1978).
43. Coenen, J. W. E., *Appl. Catal.* **54**, 65 (1989).
44. Hoang-Van, C., Kachaya, Y., Teichner, S. J., Arnaud, Y., and Dalmon, J. A., *Appl. Catal.* **46**, 281 (1989).
45. Halchev, T., and Ruckenstein, E., *J. Catal.* **73**, 171 (1982).
46. Falconer, J. L., and Schwartz, J. A., *Catal. Rev.–Sci. Eng.* **25**, 141 (1983).
47. Hu, Y. H., and Ruckenstein, E., *J. Catal.* **163**, 306 (1996).
48. Hadjiivanov, K., Mihaylov, M., Klissurski, D., Stefanov, P., Abadjieva, N., Vassileva, E., and Mintchev, L., *J. Catal.* **185**, 314 (1999).
49. Mihaylov, M., Hadjiivanov, K., and Knozinger, H., *Catal. Lett.* **76**, 59 (2001).
50. Carriat, J.-Y., Lepetit, C., Kermarec, M., and Che, M., *J. Phys. Chem. B* **102**, 3742 (1998).
51. Vannice, M. A., and Garten, R. L., *J. Catal.* **56**, 236 (1979).
52. Bartholomew, C. H., Pannell, R. B., and Butler, J. L., *J. Catal.* **65**, 335 (1980).
53. Arena, F., Frusteri, F., and Parlmaliana, A., *Appl. Catal. A* **187**, 127 (1999).
54. Vasquez, N., Muscat, A., and Maddix, R. J., *Surf. Sci.* **301**, 83 (1994).
55. Ofner, H., and Zaera, F., *J. Phys. Chem. B* **101**, 9069 (1997).
56. Tahri, A., Amariglio, A., and Amariglio, H., *J. Chim. Phys.* **92**, 173 (1995).
57. Bradford, M. C. J., and Vannice, M. A., *J. Catal.* **142**, 73 (1996).
58. Diaz, A., Acosta, D. R., Odriozola, J. A., and Montes, M., *J. Phys. Chem. B* **101**, 1782 (1997).
59. Arena, F., Chuvilin, A. L., and Parmaliana, A., *J. Phys. Chem.* **99**, 990 (1995).
60. Menini, C., Park, C., Brydson, R., and Keane, M. A., *J. Phys. Chem. B* **104**, 4281 (2000).
61. Somorjai, G. A., *in* "Bonding Energetics in Organometallic Compounds" (T. J. Marks, Ed.), ACS Symposium Series, Vol. 248, p. 218. Am. Chem. Soc., Washington, DC, 1990.
62. Park, C., and Baker, R. T. K., *J. Catal.* **179**, 361 (1998).
63. Cullis, C. F., Manton, J. E., Thomas, G. B., and Wilman, H., *Acta. Crystallogr.* **12**, 382 (1959).
64. Verderone, R. J., Pieck, C. L., Sad, M. R., and Parera, J. M., *Appl. Catal.* **21**, 329 (1986).
65. Chambers, A., and Baker, R. T. K., *J. Phys. Chem. B* **101**, 1621 (1997).
66. McMurry, J., "Organic Chemistry." Brooks/Cole, Pacific Grove, CA, 1992.
67. Tavoularis, G., and Keane, M. A., *J. Mol. Catal. A* **142**, 187 (1999).
68. Shin, E.-J., and Keane, M. A., *J. Chem. Technol. Biotechnol.* **75**, 159 (2000).
69. Frimmel, J., and Zdrazil, M., *J. Catal.* **167**, 286 (1997).
70. Kim, D. I., and Allen, D. T., *Ind. Eng. Chem. Res.* **36**, 3019 (1997).
71. Hagh, B., and Allen, D., *Chem. Eng. Sci.* **45**, 2695 (1990).
72. Menini, C., Tavoularis, G., Park, C., and Keane, M. A., *Catal. Today* **62**, 355 (2000).
73. Keane, M. A., and Murzin, D. Yu, *Chem. Eng. Sci.* **56**, 3185 (2001).
74. Satterfield, C. H., "Heterogeneous Catalysis in Industrial Practice," 2nd ed. McGraw–Hill, New York, 1991.